

Angular dependence, blackness and polarization effects in integral conversion electron Mössbauer spectroscopy

Szilárd Sajti,^{*} Ferenc Tanczikó, László Deák, Dénes L. Nagy, and László Bottyán
Wigner RCP, RMKI, P.O. Box 49, H-1525, Budapest, Hungary

General expressions of the electron yield in ^{57}Fe integral conversion electron Mössbauer spectroscopy were derived depending on the glancing angle of the γ photons, on the source polarization and on the isotopic abundance of the source and the absorber (blackness effects) using an exponential escape function of the electrons originating from all Mössbauer-resonance-related processes. The present approach provides a firm theoretical basis to determine the alignment and direction of magnetization in the absorber. The intensity formulae were justified by least squares fits of α - ^{57}Fe spectral intensities measured in linearly and elliptically polarized source and absorber geometries. The fits reproduce the experimentally set angles with high accuracy. Limits of the current approach and its relation to other, less complete treatments in the literature are discussed.

PACS numbers: 33.45.+x, 87.64.kx, 95.75.Hi

I. INTRODUCTION

Mössbauer spectroscopy has been very successful in determination of the alignment and direction of magnetization of buried layers of Fe, the line intensities being dependent on the angle between the propagation direction of the γ photons from the source and the hyperfine field. Using linearly polarized source we may determine alignment, and, using circularly polarized radiation, also the sign of the magnetization component parallel to the propagation direction^{1,2}. For this reason polarized Mössbauer sources were prepared^{3,4}. The so-called filter technique⁴ provides almost single-line circularly polarized radiation, resulting in relatively simple spectra, but uses only a small part of the source intensity. Application of a split multi-line source¹⁻³, however, results in more complex spectra, but provides higher intensity.

Due to the relatively shallow escape depth of the conversion electrons, of typically 5–10 keV initial energy, conversion electron Mössbauer spectroscopy (CEMS) is used for surface and thin film investigations. Not even in the case of homogeneous magnetization are conventional (perpendicular incidence) CEMS experiments appropriate to determine an arbitrary direction of the magnetization. The relative intensities do not depend on the alignment of the magnetization within the sample plane, a frequent case with thin films, in which the shape anisotropy constraints the magnetization in the sample plane.

The theoretical description of transmission Mössbauer spectroscopy is available for quite general cases. However, in a CEMS experiment, the electron transport from the Mössbauer nucleus to the sample surface is rather complex which renders the calculation of the electron yield difficult. There exist semi-empirical formulae (based on Monte-Carlo simulations) providing the probability of the escape of an electron emitted with a given energy at a given depth below the surface⁵, which can be built into the numerical algorithms, but seemingly do not allow analytical solutions, which would provide more thorough insight. As a result, most spectroscopists, when

evaluating CEM spectra, neglect the use of such escape functions and assume that the sample is very thin. In case of perpendicular-incidence and non-enriched samples, this may be justified, unlike for tilted incidence and for absorbers enriched in the Mössbauer-active isotope, when polarization- and angle-dependent blackness effects are appreciable. Even from otherwise quite general treatments of multilayer structures, e.g. Ref. 6 discussion of polarization and blackness effects are missing. Papers that qualitatively elaborate such effects, e.g. Ref. 7, leave room for improvement in regard of generality and mathematical thoroughness. The opposite extreme is the grazing incidence (approximately below 3°) CEM spectroscopy⁸, for which the theory is well established, but, as we shall see, at such angles, a different approximation of the theory applies. Moreover, experimental feasibility of grazing incidence CEMS using radioactive sources is quite limited due to the fact, that the intensity is distributed in the complete solid angle, which enables the use of less than a fraction of $\approx 10^{-5}$ of the source's activity.

In the last decade several instruments and methods were devised in our laboratory for CEM polarimetry at arbitrary (except grazing) angle of incidence and linear as well as elliptical polarization⁹⁻¹¹. The analysis of the measured spectra with these setups lead us to recognize, that treatment of the blackness effect and polarization of the radiation in the literature for conversion electron Mössbauer spectroscopy at small glancing angles and of enriched samples in the resonant isotope is not satisfactory¹⁰. The present paper tries to fill this gap. Here we derive the CEM spectral intensity in case of polarized (Mössbauer) sources, when the γ photons fall on a homogeneously magnetized sample at arbitrary (except for grazing) angle of incidence. We will discuss in detail, under what conditions conversion electron absorption effects should be accounted for and, correspondingly, whether or not blackness effect will significantly influence the resonance line intensities and widths. In particular, for ^{57}Fe CEM spectroscopy, we will show that, due to

the limited escape depth of conversion electrons, CEM samples, even those prepared from enriched ^{57}Fe , can always be treated in the thin-sample limit, as long as the incidence of resonant photons is nearly perpendicular. Conversely, for low- (but not grazing-) angle incidence an effective thickness can be introduced so that CEM spectra correspond to transmission spectra measured on resonant samples of this effective thickness if the resonance line polarization is properly taken into account in both cases.

II. CEM SPECTRA WITH THE POLARIZED γ PHOTONS INCIDENT ON THE ABSORBER AT AN ARBITRARY ANGLE

In the following, concerning nuclear resonance we will follow the theoretical considerations used in Ref. 12. Here the case of a single, homogeneous layer will be considered. Generalization for multilayers is straightforward (see Appendix A).

The number of detected electrons created by a photon beam of energy E may be written as:

$$\mathcal{N}_{\text{CE}}(D, E) \propto \int_0^D \text{Tr} \left(\bar{\rho}(z, E) N(z) \bar{\sigma}^M(z, E) \right) W(z) dz, \quad (1)$$

where D is the sample thickness, $\bar{\rho}(z)$ is the density matrix of the photons at a depth z , N is the density of the scattering centres, $\bar{\sigma}$ is the absorption cross section tensor and upper index M indicates the nuclear (Mössbauer) contribution to the quantity. $W(z)$ is the probability of a conversion electron to be emitted following the absorption of an incoming photon at depth z provided that it reaches the surface of the sample. In the case of *differential CEMS* (DCEMS) one should write $W(z, E_e)$, where E_e is the energy of the emitted electron, and $W(z, E_e)$ is the escape probability of an electron being emitted with energy E_e ¹³. For brevity, unless it may lead to misunderstanding, we will omit the energy dependence in the formulae.

The transfer operator $\bar{T}(z)$ defined by

$$|\psi(z)\rangle = \bar{T}(z) |\psi(0)\rangle \quad (2)$$

determines the wave at a depth z from the wave $|\psi(z=0)\rangle$ at the surface. Accordingly, for the density matrix we get

$$\bar{\rho}(z) = \bar{T}(z) \bar{\rho}(0) \bar{T}^\dagger(z), \quad (3)$$

where \bar{T}^\dagger denotes the Hermitian adjoint operator of \bar{T} . After some permutation and substitution we may write

$$\mathcal{N}_{\text{CE}}(D, E) \propto \text{Tr} \left(\bar{\rho}(0, E) \bar{J}(D, E) \right), \quad \text{where} \quad (4)$$

$$\bar{J}(D, E) = \int_0^D \bar{T}^\dagger(z, E) \bar{\sigma}^M(z, E) \bar{T}(z, E) N(z) W(z) dz. \quad (5)$$

For a single homogeneous layer $\bar{T}(z)$ has the following form¹⁴ (see also Appendix B):

$$\begin{aligned} \bar{T}(z) = & \cosh(ik_0 \bar{m} z \sin \vartheta) (\bar{I} + \bar{R}) \\ & + \sinh(ik_0 \bar{m} z \sin \vartheta) \bar{m}^{-1} (\bar{I} - \bar{R}), \end{aligned} \quad (6)$$

where k_0 is the wave number in vacuum, ϑ is the glancing angle of the incoming γ -beam, \bar{I} denotes the unity matrix, $|\psi_{\text{Reflected}}(0)\rangle = \bar{R} |\psi(0)\rangle$ is the reflected wave (with \bar{R} being the reflectivity tensor) at the surface of the sample. Here we introduced the tensor quantity \bar{m} with the definition

$$\bar{m} = \sqrt{\bar{I} + \frac{1}{\sin^2 \vartheta} \bar{\chi}}, \quad (7)$$

where $\bar{\chi}$ is the dielectric susceptibility tensor. For large glancing angles ϑ , the reflected beam for γ photons is weak, i.e. \bar{R} is negligible compared to the unity matrix. Consequently

$$\begin{aligned} \bar{T}(z) = & \cosh(ik_0 \bar{m} z \sin \vartheta) + \sinh(ik_0 \bar{m} z \sin \vartheta) \bar{m}^{-1} \\ = & e^{ik_0 \bar{m} z \sin \vartheta} + \sinh(ik_0 \bar{m} z \sin \vartheta) (\bar{m}^{-1} - \bar{I}). \end{aligned} \quad (8)$$

For multilayers the resulting transfer matrix is the product of single layer \bar{T} matrices of form (8). For nearly perpendicular-incidence ($\vartheta \approx \frac{\pi}{2}$) the matrix \bar{m} will be the index of refraction matrix $\bar{n} = \sqrt{\bar{I} + \bar{\chi}} \approx \bar{I} + \frac{1}{2} \bar{\chi}$. Since the dielectric susceptibility for γ photons is always small, the inverse of the index of refraction matrix is also close to the unity matrix, $\bar{n}^{-1} \approx \bar{I}$, which leads to the approximation given in Ref. 15, namely:

$$\bar{T}(z) \approx e^{ik_0 \bar{n} z} \approx e^{ik_0 z} e^{i \frac{1}{2} k_0 \bar{\chi} z}. \quad (9)$$

For small glancing angles the approximation (9) is not valid. We may expand, however, \bar{m} and \bar{m}^{-1} into Taylor-series:

$$\begin{aligned} \bar{m} = & \bar{I} + \frac{1}{2 \sin^2 \vartheta} \bar{\chi} - \frac{1}{8 \sin^4 \vartheta} \bar{\chi}^2 + \dots \\ \bar{m}^{-1} = & \bar{I} - \frac{1}{2 \sin^2 \vartheta} \bar{\chi} + \frac{3}{8 \sin^4 \vartheta} \bar{\chi}^2 + \dots \end{aligned} \quad (10)$$

In first order we get

$$\bar{T}(z) \approx e^{ik_0 z \sin \vartheta} e^{\frac{1}{2} k_0 \bar{\chi} \frac{z}{\sin \vartheta}} + \sinh(ik_0 \bar{m} z \sin \vartheta) (\bar{m}^{-1} - \bar{I}). \quad (11)$$

Higher-order terms are negligible if the eigenvalues of $\bar{\chi}$ fulfill the condition $|\chi_i| < \sin^2 \vartheta$. For ^{57}Fe on resonance ($|\chi_i| \lesssim 0.01$), therefore the first-order approximation is valid down to about $\vartheta \approx 3-5^\circ$.

Unless for very small angles, $\bar{m} \approx \bar{I}$ and therefore $\bar{m}^{-1} \approx \bar{I}$. Since in the following, we will not consider grazing incidence and will limit our considerations to $\vartheta \gtrsim 3^\circ$,

we can neglect the second term $\sinh(\dots)(\bar{\bar{m}}^{-1} - \bar{\bar{l}})$ on the right side of (11).

The absorption cross-section tensor for a single atom (molecule, etc.) can be defined as^{8,16}

$$\bar{\sigma} = -\frac{ik_0}{2N} (\bar{\chi} - \bar{\chi}^\dagger) \approx -\frac{ik_0}{N} (\bar{n} - \bar{n}^\dagger). \quad (12)$$

In the following we assume, that the electronic contribu-

tion to the susceptibility χ^e is isotropic and independent of the energy around the resonance, therefore

$$\bar{\chi}(E) = \bar{\chi}^M(E) + \chi^e \bar{\bar{l}}. \quad (13)$$

Substituting (12) and the first term of (11) into (5), the CEMS intensity matrix $\bar{\bar{J}}$ for a homogeneous layer becomes:

$$\begin{aligned} \bar{\bar{J}}(D) &= - \int_0^D e^{-i\frac{1}{2}k_0(\chi^{e*} - \chi^e) \frac{z}{\sin\vartheta}} e^{-i\frac{1}{2}k_0\bar{\chi}^{M\dagger} \frac{z}{\sin\vartheta}} \frac{ik_0}{2} (\bar{\chi}^M - \bar{\chi}^{M\dagger}) e^{i\frac{1}{2}k_0\bar{\chi}^M \frac{z}{\sin\vartheta}} W(z) dz \\ &= - \sin\vartheta \int_0^D W(z) e^{-N\sigma^e \frac{z}{\sin\vartheta}} \frac{\partial}{\partial z} \left(e^{-i\frac{1}{2}k_0\bar{\chi}^{M\dagger} \frac{z}{\sin\vartheta}} e^{i\frac{1}{2}k_0\bar{\chi}^M \frac{z}{\sin\vartheta}} \right) dz, \end{aligned} \quad (14)$$

where $*$ denotes complex conjugation. Introducing the $s = i\frac{1}{2}k_0z/\sin\vartheta$ notation and using the Baker–Campbell–Hausdorff formula¹⁷ the product of the two matrix exponentials can be written as

$$\begin{aligned} e^{-s\bar{\chi}^{M\dagger}} e^{s\bar{\chi}^M} &= e^{s(\bar{\chi}^M - \bar{\chi}^{M\dagger}) - \frac{1}{2}s^2[\bar{\chi}^{M\dagger}, \bar{\chi}^M]} \\ &\quad + \frac{1}{12}s^3[\bar{\chi}^M - \bar{\chi}^{M\dagger}, [\bar{\chi}^{M\dagger}, \bar{\chi}^M]] + \dots \end{aligned} \quad (15)$$

For the M1 nuclear transitions, like in ^{57}Fe , for almost all practical cases the $[\bar{\chi}^M, \bar{\chi}^{M\dagger}] = 0$ condition is fulfilled with a good approximation¹⁸. Otherwise one has to estimate the contribution of higher-order commutator terms in (15). In the following, we assume that $[\bar{\chi}^M, \bar{\chi}^{M\dagger}] = 0$ is fulfilled, therefore we have

$$\begin{aligned} \bar{\bar{J}}(D, E) &= \\ &= - \sin\vartheta \int_0^D W(z) e^{-N\sigma^e \frac{z}{\sin\vartheta}} \frac{\partial}{\partial z} e^{-N\bar{\sigma}^M(E) \frac{z}{\sin\vartheta}} dz \end{aligned} \quad (16)$$

$$= \int_0^D W(z) N\bar{\sigma}^M(E) e^{-N(\sigma^e \bar{\bar{l}} + \bar{\sigma}^M(E)) \frac{z}{\sin\vartheta}} dz. \quad (17)$$

Not regarding the number of approximations we had to make in order to obtain eq. (16), the result may seem to be commonsensical: the $\sin\vartheta$ term in front of the integral simply takes the reduced cross section of a tilted sample into account. The number of resonantly absorbed photons at depth z is given by the derivative term inside the integral. For small angles, the photons travel a longer path $z/\sin\vartheta$ to reach depth z and therefore they get absorbed more likely near the surface as compared to the case of perpendicular-incidence. However, one should keep in mind, that eq. (16) is only valid for not too small angles, when the linear approximation in eq. (11) is valid and the reflection is negligible and $[\bar{\chi}^M, \bar{\chi}^{M\dagger}] = 0$.

Until now we did not take an essential feature of the Mössbauer effect into account, namely the moving

source. The density matrix of the γ -beam emitted by the Mössbauer source that moves with velocity v can be written as

$$\begin{aligned} \bar{\rho}(z=0, E, v) &= \sum_i \bar{\rho}_i^{\text{pol}} \mathcal{L}_i(E, v) \\ &= \sum_i \bar{\rho}_i^{\text{pol}} \frac{\Gamma}{2\pi} \frac{1}{(E - E_i + \frac{v}{c}E_i)^2 + \frac{\Gamma^2}{4}}, \end{aligned} \quad (18)$$

where $\bar{\rho}_i^{\text{pol}}$ characterizes the intensity ratio and polarization of the i -th line at position E_i in the energy spectrum, $\mathcal{L}_i(E, v)$ is the (Lorentzian) shape function of the i -th line, Γ is the line width and c is the speed of light. Disregarding the background the measured CEMS intensity, as a function of the energy, i.e. of the Mössbauer drive velocity can be written as:

$$I_{\text{CEMS}}(D, v) = f_S \mathcal{I} \sum_i \text{Tr} \left(\bar{\rho}_i^{\text{pol}} \int \mathcal{L}_i(E, v) \bar{\bar{J}}(D, E) dE \right), \quad (19)$$

where f_S is Mössbauer–Lamb factor of the source and \mathcal{I} is the total intensity of the source incident on the sample.

In order to calculate the CEM spectra the knowledge of the electron escape function $W(z)$ is required. In the following, we consider ^{57}Fe CEM spectroscopy. The same treatment may be applied to CEMS on other isotopes. Liljequist derived semi-empirical formulae based on his Monte-Carlo simulations^{5,19}. Instead of depth, he used the ‘equivalent depth in iron’ defined as

$$t = \frac{\varrho}{\varrho_{\text{Fe}}} z, \quad (20)$$

where ϱ is the density of the sample and ϱ_{Fe} the density of natural iron at ambient conditions. For a homogeneous layer, the escape function can be well approximated with an exponential,

$$W(z) = W_0 e^{-\frac{t(z)}{\tau}} = W_0 e^{-z \frac{\varrho}{\varrho_{\text{Fe}} \tau}} = W_0 e^{-\frac{z}{\zeta(\varrho)}}, \quad (21)$$

where $W_0 \approx 1.155$ and $\tau \approx 540$ FeÅ. The more general escape functions are shown in Appendix C. The exponential approximation is advantageous in the parameter fitting routines, since the computer code based on the exponential escape function is by two orders of magnitude faster than the one based on exact formulae, while providing a rather good approximation. Moreover, the exponential approximation is easier to handle analytically in some special cases. Indeed, with (17) and neglecting σ^{e20} , we have

$$I_{\text{CEMS}}(D, v) = a \sum_i \text{Tr} \left[\bar{\rho}_i^{\text{pol}} \int \mathcal{L}_i(E, v) \zeta N \bar{\sigma}^M(E) \sin \vartheta \right. \\ \left. \times \left(\zeta N \bar{\sigma}^M(E) + \bar{1} \sin \vartheta \right)^{-1} \left(\bar{1} - e^{-D \left(\frac{N \bar{\sigma}^M(E)}{\sin \vartheta} + \frac{1}{\zeta} \bar{1} \right)} \right) \mathbf{E} \right], \quad (22)$$

where $a = W_0 f_S \mathcal{I}$.

First let us consider the unpolarized case. Applying the formula of effective thickness as $t = D \rho / \rho_{\text{Fe}} = DN/N_{\text{Fe}}$, and similarly $\tau = \zeta N/N_{\text{Fe}}$ and the absorption coefficient (for natural iron at ambient conditions) as $\alpha^M = N_{\text{Fe}} \sigma^M$, the exponent in eq. (22) can be transformed as follows:

$$-D \left(\frac{N \sigma^M(E)}{\sin \vartheta} + \frac{1}{\zeta} \right) = -\alpha^M t \frac{\tau \alpha^M + \sin \vartheta}{\tau \alpha^M \sin \vartheta}. \quad (23)$$

It may be convenient to interpret the quantity

$$t'(E, \vartheta) = t \frac{\tau \alpha^M(E) + \sin \vartheta}{\tau \alpha^M(E) \sin \vartheta} \quad (24)$$

as a corrected effective thickness¹⁰.

In the polarised case for small angles ($\sin \vartheta \approx 0$) we have $\zeta N \bar{\sigma}^M(E) \left(\zeta N \bar{\sigma}^M(E) + \bar{1} \sin \vartheta \right)^{-1} \approx \bar{1}$ and therefore

$$I_{\text{CEMS}}(D, v) = a \sin \vartheta \left[\bar{1} - \sum_i \text{Tr} \left(\bar{\rho}_i^{\text{pol}} \int \mathcal{L}_i(E, v) \right. \right. \\ \left. \left. \times e^{-N \bar{\sigma}^M(E) \frac{D}{\sin \vartheta}} \mathbf{E} \right) \right], \quad (25)$$

which formally corresponds to the thick sample case in absorption Mössbauer spectroscopy, as it was conjectured in Ref. 7. We should not forget, however, that beside the above mentioned constraints in deriving (16) and (22), this approximation is not valid for grazing angles, when the reflections due to the electronic contribution to the susceptibility are not negligible.

At nearly perpendicular-incidence, when $\sin \vartheta \approx 1$ we expand the exponent in Taylor series up to the second order:

$$\left(\bar{1} - e^{-D \left(N \bar{\sigma}^M(E) + \frac{1}{\zeta} \bar{1} \right)} \right) \approx \\ D \left(N \bar{\sigma}^M(E) + \frac{1}{\zeta} \bar{1} \right) + \frac{1}{2} D^2 \left(N \sigma_i^M(E) + \frac{1}{\zeta} \right)^2 + \dots \quad (26)$$

In case the second term is negligible compared to the first one, i.e.

$$\frac{1}{2} D^2 \left(N \sigma_i^M(E) + \frac{1}{\zeta} \right)^2 \ll D \left(N \sigma_i^M(E) + \frac{1}{\zeta} \right), \quad (27)$$

where σ_i is the i -th eigenvalue of $\bar{\sigma}$, and therefore the intensity expression is

$$I_{\text{CEMS}}(D, v) = a D \sum_i \text{Tr} \left(\bar{\rho}_i^{\text{pol}} \int N \bar{\sigma}^M(E) \mathcal{L}_i(E, v) \mathbf{E} \right), \quad (28)$$

which formally corresponds to the thin sample case in Mössbauer spectroscopy, as discussed in Ref. 7.

From the above, the condition of the thin absorber limit in perpendicular-incidence is

$$D \ll \frac{2}{N \sigma_{\text{max}}^M + \frac{1}{\zeta}}, \quad (29)$$

where σ_{max}^M is the maximum eigenvalue of the absorption cross section tensor. This condition means, that D is the characteristic information depth of the surface of the sample for CEM spectroscopy; no significant number of electrons will reach the sample surface from deeper layers of the sample and/or the photons will not reach a greater perpendicular depth in the sample.

For multilayers we may follow the same steps (see Appendix A), the main difference and question will be the electron escape function, which may become quite complex. The conversion electrons emitted from atoms in different layers should be summed up, taking into account the proper escape function(s), which probably may be determined as some examples of Ref. 6 show, but this is out of the scope of the present paper.

III. THICK SOURCE CASE

Blackness effects in Mössbauer spectroscopy are not limited to the absorber. Due to the possible self-absorption of the emitted photons, additional broadening may arise²¹ or, in case of a split multi-line source, the relative intensities of the emitted lines of the Mössbauer source may considerably be modified, provided that γ -emission occurs relatively deep below the surface of the source and the substrate of the source contains large amount of the resonant isotope. In the commercial Mössbauer sources the precursor of the resonant isotope is diffused into the surface layer of the substrate. When using such sources in perpendicular emission geometry, blackness effect rarely occur. However, the relative intensities of a split multiline source of α -Fe substrate at tilted exit of the γ photons, which is studied experimentally and discussed below are considerably modified by the blackness effects. In the following, we discuss the case of the thick source.

Following the same logic as in deriving (3), the density matrix of the photons emitted by the Mössbauer source may be written as

$$\bar{\rho}(E) \propto \int_0^{D_s} \bar{\mathcal{T}}(z, D_s - z, E) \bar{\sigma}^M(E) \bar{\mathcal{T}}^\dagger(z, D_s - z, E) \mathcal{N}_s(z) dz, \quad (30)$$

where D_s is the physical thickness of the substrate of the source and $\mathcal{N}_s(z)$ is the number of the nuclei emitting the resonant photons at depth z , $\bar{\mathcal{T}}(z, D_s - z)$ is the transfer operator for the source from depth z through a layer of thickness $D_s - z$ to the surface of the Mössbauer source. Generally, the source may not be regarded as a homogeneous layer in this case. Therefore $\bar{\mathcal{T}}$ should be calculated somewhat differently, than $\bar{\mathcal{T}}$ in (8). In principle it may be derived as a product of $\bar{\mathcal{T}}$ matrices of consecutive infinitesimally thin layers. In the present case, it may be assumed, that $\bar{\chi}^M$ only changes due to the density, the number $\mathcal{N}_{57\text{Fe}}$ of resonantly absorbing iron changes, i.e. $\bar{\chi}_s^M(z) = \bar{\chi}_0^M \mathcal{N}_{57\text{Fe}}(z) / (\int_0^{D_s} \mathcal{N}_{57\text{Fe}}(z) dz)$, where $\bar{\chi}_0^M$ is the average susceptibility in the sample. In that case, instead of such a product we may express $\bar{\mathcal{T}}$ using the only the first exponential terms in formulae (11), i.e. $\bar{\mathcal{T}}(z) \approx e^{ik_0 z \sin \vartheta} e^{i\frac{1}{2}k_0 \bar{\chi} \frac{z}{\sin \vartheta}}$ available for homogeneous layers, from which we get:

$$\bar{\mathcal{T}}(z, D_s - z) = e^{ik_0(D_s - z) \sin \vartheta_s} e^{i\frac{1}{2}k_0 \chi_s^e \frac{D_s - z}{\sin \vartheta_s}} e^{i\frac{1}{2}k_0 \bar{\chi}_0^M \frac{z}{\sin \vartheta_s}}, \quad (31)$$

where ϑ_s is the tilt angle of the source, χ_s^e is the electronic contribution to the susceptibility for the source (assumed to be constant) and

$$\mathcal{Z} = \frac{\int_0^{D_s} \mathcal{N}_{57\text{Fe}}(z) dz}{\int_0^{D_s} \mathcal{N}_{57\text{Fe}}(z) dz} D_s. \quad (32)$$

Due to the preparation procedure, it is correct to assume that $\mathcal{N}_s(z)$ follows a diffusion profile, i.e. an expression containing an error function.

IV. EXPERIMENTS AND THEORY

CEM polarimetric experiments were performed using α -iron foils, a natural Fe foil of 15 μm thickness as the substrate of the $^{57}\text{Co}(\alpha\text{-Fe})$ source and a ^{57}Fe foil of 20 μm thickness as the sample. A detailed description of these experiments was published in Ref. 10. The experimental spectra are the same here as in Ref. 10, but here we use a different model function. The emphasis here is being on the verification of the theory derived in the present paper.

Linear polarimetric experiments were performed in perpendicular-incidence geometry, in which the external

magnetic fields on the source (270 mT) and on the sample (400 mT) were magnetized perpendicular to the propagation direction. The results of two such measurements are shown in Fig. 1. where the magnetic fields on the source and sample are parallel and perpendicular to each other, respectively.

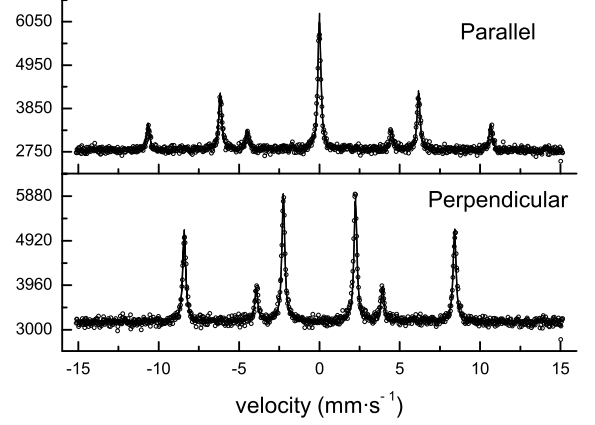


FIG. 1. Results of linear polarimetric measurements (circles) and their fits (full lines) with parallel and perpendicular source and sample magnetizations. The γ -beam is perpendicular to the plane of the source and of the sample. The magnetizations are constrained in the plane of the source and sample, respectively.

Elliptical (close to circular) polarimetric experiments were performed with a tilted source and a tilted sample, both magnetized close to their planes the magnetization vectors and the wave vector laying in the same plane. Their planes enclosed $\vartheta_s = 10^\circ$ (source) and $\vartheta = 5^\circ$ (sample) with the propagation direction. The results of two such CEM experiments are shown in Fig. 2. where the external magnetic fields on the source (230 mT) and on the sample (100 mT) were parallel and antiparallel to each other, respectively.

Having implemented the theory outlined in the former sections, measured spectra were fitted using the general fitting program *FitSuite*²². The positions and intensities of the Mössbauer lines (i.e. the contribution of the resonant absorption to $\bar{\sigma}(E)$) were calculated solving the eigenvalue problem of the corresponding hyperfine Hamiltonian. The theory described in Ref. 23 and implemented in the program EFFI²⁴ were adopted in *FitSuite* and modified to include the theoretical considerations presented above, namely eq. (22).

In the linear polarimetric case the γ -beam is perpendicular to the source and sample planes, therefore no thickness and angle dependence is expected according to (28). The magnitude and orientations of the hyperfine fields (see Table I.) were found to agree quite well with the experimental values, set by the direction of the external magnetic fields. In this case, the ϑ tilt angles of the sample and source were not fitted. These spectra depend on the difference $\Delta\varphi (= \varphi_{\text{B,sample}} - \varphi_{\text{B,source}})$ of the azimuthal angles of the hyperfine fields in the sample and

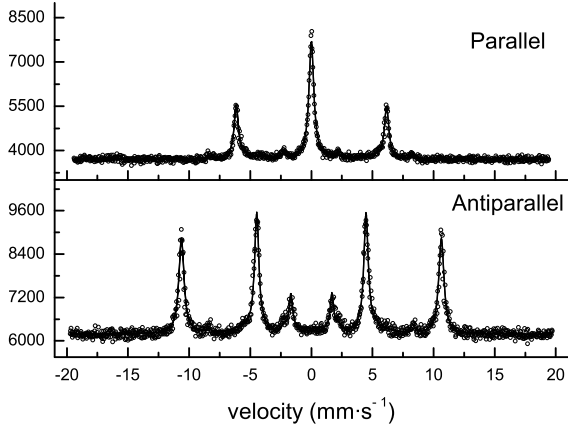


FIG. 2. Results of elliptical polarimetric measurements (circles) and their fits (full lines) with parallel and antiparallel source and sample magnetizations. The γ -beam enclosed $\vartheta_s = 10^\circ$ with the plane of the source and $\vartheta = 5^\circ$ with the sample. The external magnetic fields were parallel to the lines of intersection of the scattering plane and the planes of the sample and the source, respectively.

TABLE I. Essential fitted parameters, linear polarimetry. $\vartheta_{B,source}$ and $\vartheta_{B,sample}$ are the angles enclosed by the hyperfine field and the z axis (propagation direction of the γ photons). $\varphi_{B,source}$ and $\varphi_{B,sample}$ are the azimuthal angles measured around the z axis from the x axis being in the plane of incidence.

Parameter	Fitted	Expected
$ \mathbf{B} $	$33.05 \text{ T} \pm 0.02 \text{ T}$	–
$\vartheta_{B,source} = \vartheta_{B,sample}$	90° (fixed)	
$\varphi_{B,source}$	0° (fixed)	
Parallel case:		
$\varphi_{B,sample} - \varphi_{B,source}$	$-0.2^\circ \pm 0.8^\circ$	0°
Perpendicular case:		
$\varphi_{B,sample} - \varphi_{B,source}$	$89.8^\circ \pm 0.8^\circ$	90°

the source, therefore $\Delta\varphi$ was the fit parameter. The two spectra were simultaneously fitted using the constraint $\Delta\varphi^{\text{perpendicular}} = \Delta\varphi^{\text{parallel}} + 90^\circ$. Indeed, the perpendicular setup was obtained from the parallel one by the rotation of the source polarizer magnet by 90° . To reproduce the expected angles we had to assume that the source was not completely polarized, and that the emitted beam had a degree of polarization $P = 0.98 \pm 0.007$. As the source was not saturated (As the coercive field of bulk bcc Fe is known not to be able fully saturate in plane an alpha-Fe foil and to saturate the last few per cents magnetic fields in the order of 1 T are needed.²⁵), this is expectable, and the value of P agrees well with the value $P = 0.96$ obtained in a different experiment in Ref. 9. The partially polarized source was modelled by using an additional site in the source with orthogonal ($\varphi_{B,source} = 90^\circ$) hyperfine field of $(1 - P)/(1 + P)$ times smaller intensity than that of the ‘main component’. This results in a source spec-

trum of the desired degree of polarization and, as far as coherent scattering can be neglected, which is certainly the case as long as blackness effect plays no significant role, the contributions of different sites of the source can be added up incoherently. Indeed, according to our simulations the change of the sample thickness gives rise to the change of intensity, but the lineshape of the spectra remains unchanged.

TABLE II. Essential fitted parameters, elliptical polarimetry. $\vartheta_{B,source}$ and $\vartheta_{B,sample}$ are the angles enclosed by the hyperfine field and the z axis (propagation direction of the γ photons). $\varphi_{B,source}$ and $\varphi_{B,sample}$ are the azimuthal angles measured around the z axis from the x axis being in the plane of incidence. The magnetizations are assumed to lie in the source and sample planes, therefore (during fitting) $\vartheta_{B,sample}$ and $\vartheta_{B,source}$ were assumed to be identical with the corresponding tilt angles ϑ and ϑ_s , respectively.

Parameter	Fitted	Expected
Source tilt angle (ϑ_s)	$10.1^\circ \pm 0.7^\circ$	10°
Sample tilt angle (ϑ)	$4.97^\circ \pm 0.04^\circ$	5°
$ \mathbf{B}_{source} $	$32.866 \text{ T} \pm 0.017 \text{ T}$	–
$\vartheta_{B,source}$	$= \vartheta_s$	10°
$\varphi_{B,source}$	0° (fixed)	
$ \mathbf{B}_{sample} $	$33.082 \text{ T} \pm 0.002 \text{ T}$	–
Parallel case:		
$\vartheta_{B,sample}$	$= \vartheta$	5°
$\varphi_{B,sample}$	0° (fixed)	
Antiparallel case:		
$\vartheta_{B,sample}$	$= \vartheta$	5°
$\varphi_{B,sample}$	180° (fixed)	

This is not the case for the nearly circular polarimetric experiments, where the blackness effect plays an important role and therefore the intensity ratios strongly depend on the thickness and tilt angle, as it can be seen in Figs. 3-4. Without this effect, the intensity ratios of the spectra of Fig. 2. could not be explained either. The measured spectra and hyperfine field orientations (Table II) could be reproduced relatively well if the degree of polarization of the source was $P = 0.924 \pm 0.010$. This is worse, than in the linear polarization case, but it may be explained with the incomplete saturation by the external magnetic field of 230 mT and by the experimental geometry: tilted sample and source. The partial polarization of the source here was taken into account also by an additional site, but here its hyperfine field was chosen antiparallel (as that belongs to the orthogonal polarization). In this case, because of the thick tilted source, this may not result completely correctly the desired polarization degree, but it can be used, as in an experiment, P is just an additional calibration parameter. The experimentalist would like to determine the orientation of the magnetization in the sample.

In fitting the circular polarimetric spectra at a glancing angle of $\vartheta = 5^\circ$, when the perpendicular informa-

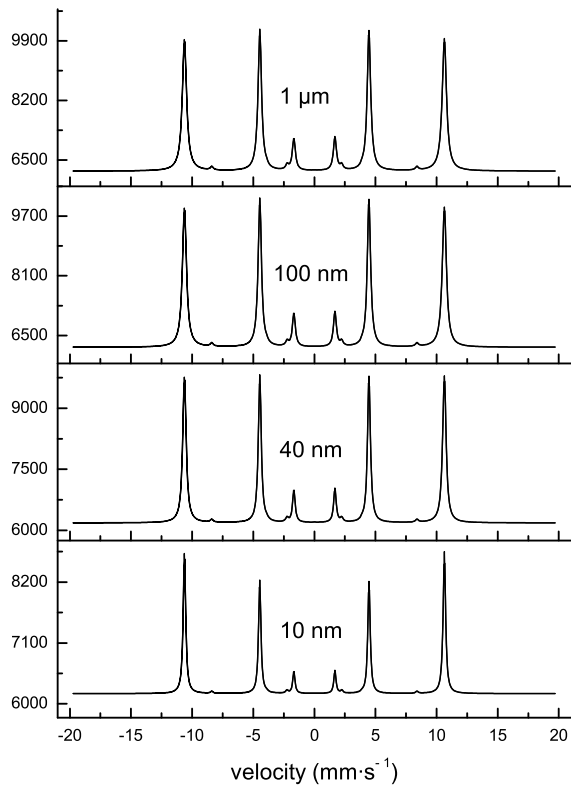


FIG. 3. Demonstration of the thickness dependence of the blackness effect. Results of elliptical polarimetric simulations with antiparallel source and sample magnetizations for different sample thicknesses ($D = 10$ nm, ..., 1 μ m). Other parameters (see Table II) are the same as in the corresponding fitted spectrum plotted in Fig. 2, but the additional site due to the superparamagnetic iron-oxide on sample surface was not taken into account and it was assumed to have a thin source.

tion depth D is much smaller, than in the perpendicular-incidence case. We had to take into account an additional singlet site with isomer shift (0.136 ± 0.070) $\text{mm} \cdot \text{s}^{-1}$, effective thickness (31.5 ± 1.9) $\text{Fe}^{57}\text{\AA}$ with Lorentzian broadening of $(17.5 \pm 1.4) \times \Gamma^{\text{nat}}$ ($\Gamma^{\text{nat}} = 0.097$ $\text{mm} \cdot \text{s}^{-1}$ is the width of the natural line broadening) which is most probably due to a small amount of superparamagnetic iron oxide on the surface of the absorber. In case of linear polarimetric measurements this component did not appear, since in perpendicular-incidence its contribution to the measured spectrum was much smaller.

The fits of elliptical polarimetric experiments, shown in Ref. 10 provided two times larger values for (ϑ_B) angles, which determine the tilt of the magnetization, than the values available here in Table II and what is expected from the experimental arrangement. This clearly shows, that, instead of the simple model used in Ref. 10, the angular dependence, blackness and polarization effects are to be taken into account in a correct evaluation of CEM spectra, as outlined above.

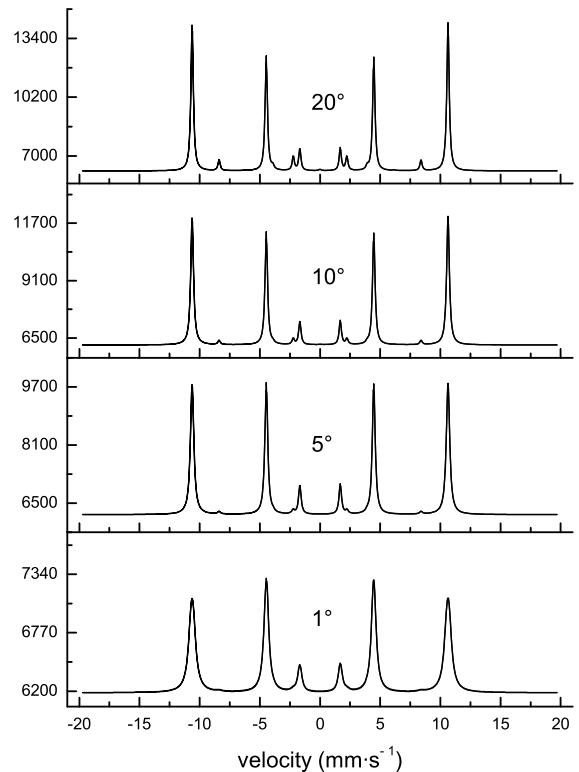


FIG. 4. Demonstration of the angular dependence of the blackness effect. Results of elliptical polarimetric simulations with antiparallel source and sample magnetizations for $D=40$ nm thick samples tilted in different angles ($\vartheta = 1^\circ$, ..., 20°). Other parameters (see Table II) are the same as in the corresponding fitted spectrum plotted in Fig. 2, but the additional site due to the superparamagnetic iron-oxide on sample surface was not taken into account and it was assumed to have a thin source.

V. SUMMARY

In this paper it was examined, how the CEM spectra may be calculated for thick tilted single or multilayer samples measured by CEM polarimetry in order to determine the magnitude and direction of layer magnetization with high accuracy. We showed, what conditions are to be fulfilled to justify the different approaches in evaluation: CEM spectra may be regarded, as transmission Mössbauer spectra (except for the change of absorption to emission lines):

- of a thin sample, if the γ photons from the source are incident on the sample at a large glancing angle or perpendicularly and the condition (29) is fulfilled;
- of a thick sample, if the γ photons from the source are incident on the sample at a small glancing angle, which is still greater than what we usually call grazing incidence.

These statements are verified for electron escape of a single exponential form. Furthermore, we may not regard the CEM spectra either as a thin or a thick Mössbauer spectrum for angles between the two limiting cases, and in case of grazing incidence. We may use for calculations the equations: (4) and (16) for intermediate angles ($3^\circ \lesssim \vartheta \leq 90^\circ$); (4), (5) and (6) in case of grazing incidence and small glancing angles ($\vartheta \lesssim 3^\circ$).

We made numerous simulations and data fitting, using the FitSuite code, and we found good agreement between theoretical and experimental results.

Appendix A: CEM spectra in case of multilayers

Let us assume a sample of n homogeneous layers, and use the following notations:

- D_i is the depth z at which the interface of the i -th and the $i + 1$ -th layer can be found, $D_0 = 0$ and $D_n = D$,
- $\bar{\bar{T}}_i(z)$ is the transfer operator in the range ($D_{i-1} \leq z \leq D_i$) of the two bounding interfaces of the i -th layer, $\bar{\bar{T}}_i(D_{i-1}) = \bar{\bar{I}}$,
- $\bar{\bar{\sigma}}_i^M$ and σ_i^e are the part of the absorption cross section tensor belonging to Mössbauer effect and the electronic contribution to the absorption cross section for the i -th layer, respectively,
- N_i is the density of the Mössbauer resonant nuclei in the i -th layer.

Using this notation the number of detected electrons may be written as:

$$\mathcal{N}_{\text{CE}}(D, E) \propto \sum_{i=1}^n \text{Tr} \left(\bar{\bar{\rho}}_i(E) \bar{\bar{J}}_i(E) \right), \quad \text{where} \quad (A1)$$

$$\bar{\bar{\rho}}_i(E) = \bar{\bar{T}}(D_{i-1}, E) \bar{\bar{\rho}}(0, E) \bar{\bar{T}}^\dagger(D_{i-1}, E)$$

$$\bar{\bar{J}}_i(E) = \int_{D_{i-1}}^{D_i} \bar{\bar{T}}_i^\dagger(z, E) \bar{\bar{\sigma}}_i^M(E) \bar{\bar{T}}_i(z, E) N_i W(z) dz.$$

Using the same approximations and omissions for $\bar{\bar{T}}_i(z)$ as in deriving eq. (16) from eq. (5) we may get

$$\bar{\bar{J}}_i(E) = -\sin \vartheta \int_{D_{i-1}}^{D_i} W(z) e^{-N_i \sigma_i^e \frac{z-D_{i-1}}{\sin \vartheta}} \times \frac{\partial}{\partial z} \left(e^{-N_i \bar{\bar{\sigma}}_i^M(E) \frac{z-D_{i-1}}{\sin \vartheta}} \right) dz. \quad (A2)$$

Applying these expressions and knowing the proper $W(z)$ escape function for the multilayer system the spectra can be calculated (provided that the approximations leading to (16) hold).

Appendix B: Transfer matrix

The form of eq. (6) is not readily available in Ref. 14. Therefore derivation of eq. (6) from formulae of Ref. 14 is presented below. According the equations (A4-A5) of Ref. 14 we have

$$\bar{\bar{T}}(z) = \bar{\bar{L}}^{[22]} (\bar{\bar{I}} + \bar{\bar{R}}) + \bar{\bar{L}}^{[21]} (\bar{\bar{I}} - \bar{\bar{R}}), \quad (B1)$$

where the 2×2 minor matrices of $\bar{\bar{L}}$ are defined in (B2) of Ref. 14, as

$$\bar{\bar{L}}^{[21]} = i \sin \vartheta \bar{\bar{F}}^{-1} \sinh(k_0 z \bar{\bar{F}}), \quad \bar{\bar{L}}^{[22]} = \cosh(k_0 z \bar{\bar{F}}), \quad (B2)$$

where $\bar{\bar{F}} = \sqrt{-\bar{\bar{I}} \sin^2 \vartheta - \bar{\bar{\chi}}}$. Using the definition (7) we may write $\bar{\bar{F}} = i \bar{\bar{m}} \sin \vartheta$, and therefore

$$\bar{\bar{L}}^{[21]} = \bar{\bar{m}}^{-1} \sinh(ik_0 z \bar{\bar{m}} \sin \vartheta), \quad \bar{\bar{L}}^{[22]} = \cosh(ik_0 z \bar{\bar{m}} \sin \vartheta). \quad (B3)$$

Substituting these minor matrices of $\bar{\bar{L}}$ into (B1) we get (6).

Appendix C: Electron escape function

The electrons are emitted as a result of several secondary processes after irradiation the sample by γ photons, which all should be taken into account in the escape functions. According to Ref. 5 the electron escape probability from a depth z can be written as:

$$W(z) = \sum_i c_i W_i(z), \quad (C1)$$

where c_i gives the contribution of the i -th process, for which the escape function is $W_i(z)$. The escape function, using the concept of the equivalent iron depth t instead of z (definition is given in (20)) for K, L-M and Auger electrons, has the form:

$$W_i(x) = \begin{cases} 0.74 - 2.7x + 2.5x^2 & \text{if } 0 \leq x \leq 0.55 \\ 0 & \text{otherwise} \end{cases}, \quad (C2)$$

where $x = \frac{t}{r_i^{\text{Bethe}}}$ and r_i^{Bethe} is the Bethe range (which is on average the total distance, which an electron travels until it gets trapped)⁵. Alternative formulae for K, L-M and Auger electrons based on Gaussian functions are available in Refs. 19 and 26:

$$W(t, E_e) = A(Z, E_e) e^{-\frac{t}{R(Z, E_e)}} e^{-\left(\frac{t}{1.9R(Z, E_e)}\right)^2}, \quad (C3)$$

where Z is the atomic number and E_e the energy with which the electron was emitted from the atom. For further details regarding the functions $A(Z, E_e)$ and $R(Z, E_e)$ see Ref. 19. To get the alternative $W_i(t)$ functions of (C2) we have to integrate $W(t, E_e)$ according

to the electron energies in the corresponding ranges too. Therefore (C3) is more appropriate for DCEMS prob-

lems, for which (C2) is completely inappropriate.

For photo-electrons the escape function has the form:

$$W_i(t) = \frac{U_{\infty i}}{r_i^{\text{eff}}} \begin{cases} 1 - 0.5 [\text{E}_2(\mu_i t) - \text{E}_2(\mu_i(r_i^{\text{eff}} - t))] & \text{if } 0 \leq t \leq r_i^{\text{eff}} \\ 0.5 [\text{E}_2(\mu_i(t - r_i^{\text{eff}})) - \text{E}_2(\mu_i t)] & \text{if } r_i^{\text{eff}} < t \end{cases}, \quad (\text{C4})$$

where $\text{E}_2(x)$ is the second-order exponential integral function defined by $\text{E}_2(x) = \int_1^\infty h^{-2} e^{-xh} dh = \int_0^1 e^{-\frac{x}{u}} \frac{1}{u^2} du$, r_i^{eff} is the so-called effective range, μ_i is absorption coefficient for the conversion photons, $U_{\infty i}$ is a normalization constant.

ACKNOWLEDGMENTS

Kind advices and helpful comments by Prof. Hartmut Spiering, Universität Mainz and financial support by Hungarian Scientific Research Fund in OTKA K62272 and T047094, and by the NAP-VEENEUS'08 project of the National Office for Research and Technology of Hungary are gratefully acknowledged.

-
- * sajti.szilard@wigner.mta.hu
- ¹ U. Gonser, R. W. Grant, H. Wiederisch, and S. Geller, *Appl. Phys. Lett.* **9**, 18 (1966).
 - ² S. Shtrikman and S. Somekh, *Rev. Sci. Instrum.* **40**, 1151 (1969).
 - ³ H. Frauenfelder, D. E. Nagle, R. D. Taylor, D. R. F. Cochran, and W. M. Wisscher, *Phys. Rev.* **126**, 1065 (1962).
 - ⁴ K. Szymański, L. Dobrzyński, B. Prus, and M. J. Cooper, *Nucl. Instr. and Meth. B* **119**, 438 (1996).
 - ⁵ D. Liljequist, T. Ekdahl, and U. Bäverstam, *Nucl. Instr. and Meth.* **155**, 529 (1978).
 - ⁶ F. Nagy and Z. Klencsár, *Nucl. Instr. and Meth. B* **245**, 528 (2006).
 - ⁷ W. Olszewski, K. Szymański, D. Satula, L. Dobrzyński, L. Bottyán, and F. Tanczikó, *Nucl. Instr. and Meth. B* **266**, 3319 (2008).
 - ⁸ S. M. Irkaev, M. A. Andreeva, V. G. Semenov, G. N. Be-lozerskii, and O. V. Grishin, *Nucl. Instr. and Meth. B* **74**, 554 (1993).
 - ⁹ F. Tanczikó, L. Deák, D. L. Nagy, and L. Bottyán, *Nucl. Instr. and Meth. B* **226**, 461 (2004).
 - ¹⁰ F. Tanczikó, S. Sajti, L. Deák, D. G. Merkel, G. Endrőczy, D. L. Nagy, L. Bottyán, W. Olszewski, and K. Szymański, *Rev. Sci. Instrum.* **81**, 023302 (2010).
 - ¹¹ F. Tanczikó, L. Bottyán, L. Deák, D. G. Merkel, and D. L. Nagy, *Hyp. Int.* **188**, 79 (2009).
 - ¹² L. Deák, L. Bottyán, D. L. Nagy, and H. Spiering, *Phys. Rev. B* **53**, 6158 (1996).
 - ¹³ D. Liljequist and M. Ismail, *Phys. Rev. B* **31**, 4131 (1985).
 - ¹⁴ L. Deák, L. Bottyán, D. L. Nagy, H. Spiering, Y. N. Khaidukov, and Y. Yoda, *Phys. Rev. B* **76**, 224420 (2007).
 - ¹⁵ M. Blume and O. C. Kistner, *Phys. Rev.* **171**, 417 (1968).
 - ¹⁶ L. Landau and E. Lifshitz, “Electrodynamics of continuous media,” (Pergamon, 1984) Chap. XI, p. 332, 2nd ed.
 - ¹⁷ E. Hairer, C. Lubich, and G. Wanner, “Geometric numerical integration: Structure-preserving algorithms for ordinary differential equations,” (Springer, 2006) Chap. III, pp. 83–87, 2nd ed.
 - ¹⁸ H. Spiering, in *Mössbauer Spectroscopy Applied to Inorganic Chemistry, Vol. 1*, Modern inorganic chemistry, edited by G. J. Long (Springer, 1984) pp. 95,99–100.
 - ¹⁹ D. Liljequist, *Nucl. Instr. and Meth. B* **142**, 295 (1998).
 - ²⁰ This usually can be done near the resonance and for the glancing angles examined here. Even if it is not the case, this exponential term could be taken into account formally just by replacing $\frac{1}{\zeta}$ with $\frac{1}{\zeta} + \frac{N\sigma^e}{\sin \vartheta}$.
 - ²¹ S. Margulies and J. R. Ehrman, *Nucl. Instr. and Meth.* **12**, 131 (1961).
 - ²² FitSuite is freely downloadable from its homepage <http://www.fs.kfki.hu>.
 - ²³ H. Spiering, L. Deák, and L. Bottyán, *Hyp. Int.* **125**, 197 (2000).
 - ²⁴ EFFI is freely downloadable from its homepage <http://ak-guetlich.chemie.uni-mainz.de/effi>.
 - ²⁵ R. Röhlberger, private communication; our unpublished results.
 - ²⁶ D. Liljequist, *Nucl. Instr. and Meth. B* **174**, 351 (2001).
 - ²⁷ M. Abramovitz and I. A. Stegun, eds., *Handbook of mathematical functions*, tenth printing ed. (Dover Publications, 1964).